SIAM J. NUMER. ANAL.
Vol. 58, No. 1, pp. 353–374

A SEQUENTIAL LEAST SQUARES METHOD FOR POISSON EQUATION USING A PATCH RECONSTRUCTED SPACE*

RUO LI† AND FANYI YANG‡

Abstract. We propose a new least squares finite element method to solve the Poisson equation. By using a piecewisely irrotational space to approximate the flux, we split the classical method into two sequential steps. The first step gives the approximation of flux in the new approximation space, and the second step can use flexible approaches to give the pressure. The new approximation space for flux is constructed by patch reconstruction with one unknown per element consisting of piecewisely irrotational polynomials. The error estimates in the energy norm and L^2 norm are derived for the flux and the pressure. Numerical results verify the convergence order in error estimates and demonstrate the flexibility and particularly the great efficiency of our method.

Key words. Poisson equation, patch reconstructed, irrotational polynomial space, discontinuous least squares finite element method

AMS subject classification. 65N30

DOI. 10.1137/19M1239593

1. Introduction. The least squares finite element method is a sophisticated technique for solving the partial differential equation. For the second-order elliptic problems, we refer the reader to [12, 22, 13, 31, 5, 30], and for the Navier–Stokes problem, we refer the reader to [10, 8, 14]. For an overview of the least squares finite element methods, we refer the reader to [11] and the references therein. Different from the Galerkin method, the least squares method is based on the minimization of the L^2-norm residual over a proper approximation space. An immediate advantage is that the resulting linear system is symmetric positive definite, which has made the method attractive in several fields. Instantly, one may see that the condition number of the resulting linear system is squared due to the formation of the approximation. To relieve the curse due to the condition number, one may write the equation into a low-order formation. Taking the Poisson equation as an example, one may introduce a flux variable to write it into the mixed formation, resulting in a system coupled by the flux and pressure [30, 7]. Though the mixed form is helpful in reducing the condition number, more degrees of freedom (DOFs) are introduced to achieve the same accuracy.

Discontinuous Galerkin (DG) methods have received pervasive attention in the past two decades due to their great flexibility in mesh partition and easy implementation of the approximation spaces, especially for the spaces of high-order accuracy. We refer the reader to the review paper [3] and the references therein. Using the approximation space from the DG methods, discontinuous least squares (DLS) finite element methods have been developed in [33, 7, 6] for solving the elliptic system. In [8, 9], the authors extend the DLS finite element methods to the Stokes problem in

*Received by the editors January 22, 2019; accepted for publication (in revised form) November 5, 2019; published electronically January 16, 2020.
https://doi.org/10.1137/19M1239593
Funding: This work was supported by National Natural Science Foundation of China grants 91630310, 11421110001, and 11421101 and Science Challenge Project grant TZ2016002.

†CAPT, LMAM, and School of Mathematical Sciences, Peking University, Beijing 100871, People's Republic of China (rli@math.pku.edu.cn).
‡School of Mathematical Sciences, Peking University, Beijing 100871, People's Republic of China (yangfanyi@pku.edu.cn).

velocity-vorticity-pressure form. The same as the least squares methods using continuous approximation space, the technique to write the equation into a low-order system is also adopted in DLS methods to reduce the condition number of resulting linear systems. To achieve the high-order accuracy, discontinuous finite element space requires a huge number of DOFs, which leads to a very large linear system [21, 34] in comparison to the methods using continuous approximation spaces. The coupling of the variables in the mixed form and the increasing of the number of DOFs make one hard to satisfy with its efficiency.

In this paper, a new least squares finite element method is proposed to solve the Poisson equation. The novel point is that we split the solver into two sequential steps. This is motivated from the idea in [6] to decouple the least squares–type functional into two subproblems. In the first step, we approximate the flux still using a discontinuous approximation space. This space is a piecewisely irrotational polynomial space, which is a generalization of the reconstructed space proposed in [27, 25]. The DG reconstruction techniques have been proposed for a variety of problems; we refer the reader to [24, 18, 16] for more details. In this paper, the new reconstructed space is obtained by solving a local least squares problem based on the irrotational polynomial bases and only one unknown locates inside each element. The piecewisely irrotational property of the new space leads to a uniquely solvable formulation for the flux, which allows us to decouple the flux and make the pressure implementable. For the flux, the optimal error estimate with respect to the energy norm is derived. We have only been able to prove the suboptimal convergence rate in the L^2 norm for the flux up until now, while in numerical experiments we observe the optimal convergence behavior for the space of odd order.

Once the numerical approximation to the flux is obtained, one then could use the numerical flux to obtain the pressure in a very flexible manner. As a demonstration, we adopt the standard C^0 finite element space to solve the pressure. We give the error estimates of the pressure in both the energy norm and the L^2 norm. By a series of numerical examples, we at first verify the convergence order given in the error estimate and illustrate the flexibility inherited from the DG method. Particularly, by the comparison [21] of the number of DOFs used to achieve the same numerical error, we show that our method has a great saving in DOFs compared to the standard DLS finite element method. Consequently, by the decoupling of the flux and the pressure, and by the saving in the number of DOFs, a much better efficiency could be attained by our method.

The rest of this paper is organized as follows. In section 2, we review the standard DLS finite element method and present the corresponding error estimates. In section 3, we introduce a reconstruction operator to define the piecewisely irrotational approximation space, and we give the approximation property of the new space. In section 4, the approximation to the flux and the pressure of the Poisson problem is proposed, and we derive the error estimates for both flux and pressure in the energy and L^2 norms. In section 5, we present the numerical examples on meshes with different geometry to verify the convergence order in the error estimates. We also give a numerical indication of the condition number of the stiffness matrix arising from the flux equation. In addition, we make a comparison of the number of DOFs with respect to the numerical error between our method and the method in section 2 to show the great efficiency of our method.

2. Discontinuous least squares finite element method. Let Ω be a bounded polygonal domain in $\mathbb{R}^d (d = 2, 3)$. Let $\mathcal{T}_h$ be a partition of Ω into polygonal (poly-

hedral) elements. We denote by $\mathcal{E}_h^i$ the set of interior element faces of $\mathcal{T}_h$ and by $\mathcal{E}_h^b$ the set of the element faces on the boundary $\partial\Omega$, and thus the set of all element faces $\mathcal{E}_h = \mathcal{E}_h^b \cup \mathcal{E}_h^i$. The diameter of an element K is denoted by $h_K = \mathrm{diam}(K)\ \forall K \in \mathcal{T}_h$, and the size of the face e is $h_e = |e|\ \forall e \in \mathcal{E}_h$. We set $h = \max_{K\in\mathcal{T}_h} h_K$. It is assumed that the elements in $\mathcal{T}_h$ are shape-regular according to the conditions specified in [1], which read as follows: There are

- two positive numbers N and σ which are independent of h;
- a compatible subdecomposition $\widetilde{\mathcal{T}}_h$ consisting of shape-regular triangles

such that

- any element $K \in \mathcal{T}_h$ admits a decomposition $\widetilde{\mathcal{T}}_{h|K}$ which is composed of less than N shape-regular triangles; and
- a shape-regular triangle $\widetilde{K} \in \widetilde{\mathcal{T}}_h$ in the sense that the ratio between $h_{\widetilde{K}}$ and $\rho_{\widetilde{K}}$ is bounded by σ: $h_{\widetilde{K}}/\rho_{\widetilde{K}} \le \sigma$, where $\rho_{\widetilde{K}}$ is the radius of the largest ball inscribed in $\widetilde{K}$.

The regularity conditions lead to some useful consequences which are easily verified:

M1 There exists a positive constant σ_s such that $\sigma_s h_K \le h_e$ for any element K and every edge e of K.

M2 [*trace inequality*] There exists a positive constant C such that

$$\|v\|^2_{L^2(\partial K)} \le C\left(h_K^{-1}\|v\|^2_{L^2(K)} + h_K\|\nabla v\|^2_{L^2(K)}\right) \quad \forall v \in H^1(K). \tag{2.1}$$

M3 [*inverse inequality*] There exists a positive constant C such that

$$\|\nabla v\|_{L^2(K)} \le C h_K^{-1}\|v\|_{L^2(K)} \quad \forall v \in \mathbb{P}_m(K), \tag{2.2}$$

where $\mathbb{P}_m(\cdot)$ is the polynomial space of degree $\le m$.

Next, we introduce the standard trace operators in the discontinuous Galerkin (DG) framework [3]. Let v and $\mathbf{q}$ be the scalar-valued and vector-valued functions, respectively. Let $e \in \mathcal{E}_h^i$ be shared by two adjacent elements K^+ and K^- with the unit outward normals $\mathbf{n}^+$ and $\mathbf{n}^-$ corresponding to ∂K^+ and ∂K^-, respectively. We define the average operator $\{\cdot\}$ and the jump operator $[\![\cdot]\!]$ as

$$\{v\} = \frac{1}{2}\left(v|_{K^+} + v|_{K^-}\right), \quad \{\mathbf{q}\} = \frac{1}{2}\left(\mathbf{q}|_{K^+} + \mathbf{q}|_{K^-}\right) \quad \forall e \in \mathcal{E}_h^i,$$

and

$$[\![v]\!] = v|_{K^+}\mathbf{n}^+ + v|_{K^-}\mathbf{n}^-, \quad [\![\mathbf{q}]\!] = \mathbf{q}|_{K^+}\cdot\mathbf{n}^+ + \mathbf{q}|_{K^-}\cdot\mathbf{n}^-,$$
$$[\![\mathbf{q}\otimes\mathbf{n}]\!] = \mathbf{q}|_{K^+}\otimes\mathbf{n}^+ + \mathbf{q}|_{K^-}\otimes\mathbf{n}^- \quad \forall e \in \mathcal{E}_h^i,$$

where $\otimes$ denotes the tensor product between two vectors. In this case, $e \in \mathcal{E}_h^b$, $\{\cdot\}$ and $[\![\cdot]\!]$ are modified as

$$\{v\} = v, \quad [\![v]\!] = v\mathbf{n}, \quad [\![\mathbf{q}]\!] = \mathbf{q}\cdot\mathbf{n}, \quad [\![\mathbf{q}\otimes\mathbf{n}]\!] = \mathbf{q}\otimes\mathbf{n} \quad \forall e \in \mathcal{E}_h^b,$$

where $\mathbf{n}$ denotes the unit outward normal to e.

Throughout the paper, let us note that C and C with a subscript are generic constants which may be different from line to line but are independent of the mesh size. We follow the standard definitions for the spaces $L^2(D)$, $H^t(D)$, $C^t(D)$, $\mathbf{L}^2(D) := [L^2(D)]^d$, $\mathbf{H}^t(D) = [H^t(D)]^d$, and $\mathbf{C}^t(D) = [C^t(D)]^d (t \ge 0)$, and we define

$$H(\mathrm{curl}^0; D) \triangleq \left\{\boldsymbol{v} \in \mathbf{L}^2(D) \mid \nabla\times\boldsymbol{v} = 0\right\}.$$

The problem considered in this article is the following Poisson equation: seek u such that

$$\begin{aligned} -\Delta u &= f \quad \text{in } \Omega, \\ u &= g \quad \text{on } \partial\Omega. \end{aligned} \tag{2.3}$$

The first step of usual least squares finite element methods [33, 7] is to write the problem (2.3) into an equivalent mixed form: seek $\mathbf{p}$ and u such that

$$\begin{aligned} \mathbf{p} - \nabla u &= \mathbf{0} \quad \text{in } \Omega, \\ -\nabla \cdot \mathbf{p} &= f \quad \text{in } \Omega, \\ u &= g \quad \text{on } \partial\Omega. \end{aligned} \tag{2.4}$$

In the mixed form, we refer to u as the pressure and $\mathbf{p}$ as the flux later on based on the terminology of the background of this equation in fluid dynamics [30, 7]. Here we introduce two discontinuous approximation spaces, V_h^m for the pressure u and $\mathbf{W}_h^m$ for the flux $\mathbf{q}$, which are defined as follows:

$$\begin{aligned} V_h^m &= \left\{ v_h \in L^2(\Omega) \mid v_h|_K \in \mathbb{P}_m(K) \ \forall K \in \mathcal{T}_h \right\}, \\ \mathbf{W}_h^m &= \left\{ \mathbf{q}_h \in \mathbf{L}^2(\Omega) \mid \mathbf{q}_h|_K \in [\mathbb{P}_m(K)]^d \ \forall K \in \mathcal{T}_h \right\}, \end{aligned}$$

where m is a positive integer. We equip these two approximation spaces with the following norms, $\|\cdot\|_u$ for V_h^m and $\|\cdot\|_{\mathbf{p}}$ for $\mathbf{W}_h^m$, respectively, as

$$\begin{aligned} \|v_h\|_u^2 &\triangleq \sum_{K\in\mathcal{T}_h} \|\nabla v_h\|_{L^2(K)}^2 + \sum_{e\in\mathcal{E}_h} h^{-1} \|[\![v_h]\!]\|_{L^2(e)}^2 \quad \forall v_h \in V_h^m, \\ \|\mathbf{q}_h\|_{\mathbf{p}}^2 &\triangleq \sum_{K\in\mathcal{T}_h} \left(\|\nabla \cdot \mathbf{q}_h\|_{L^2(K)}^2 + \|\mathbf{q}_h\|_{L^2(K)}^2 \right) + \sum_{e\in\mathcal{E}_h^i} h^{-1} \|[\![\mathbf{q_h}]\!]\|_{L^2(e)}^2 \quad \forall \mathbf{q}_h \in \mathbf{W}_h^m. \end{aligned}$$

The standard least squares finite element method based on mixed form (2.4) [33, 7] reads as follows: find $(u_h, \mathbf{p}_h) \in V_h^m \times \mathbf{W}_h^m$ such that

$$J_h(u_h, \mathbf{p}_h) = \inf_{(v_h,\mathbf{q}_h)\in V_h^m \times \mathbf{W}_h^m} J_h(v_h, \mathbf{q}_h), \tag{2.5}$$

where $J_h(\cdot,\cdot)$ is the least squares functional which is defined as

$$\begin{aligned} J_h(v_h, \mathbf{q}_h) \triangleq & \sum_{K\in\mathcal{T}_h} \left(\|\nabla \cdot \mathbf{q}_h + f\|_{L^2(K)}^2 + \|\nabla v_h - \mathbf{q}_h\|_{L^2(K)}^2 \right) \\ & + \sum_{e\in\mathcal{E}_h^i} \frac{1}{h} \|[\![v_h]\!]\|_{L^2(e)}^2 + \sum_{e\in\mathcal{E}_h^i} \frac{1}{h} \|[\![\mathbf{q}_h]\!]\|_{L^2(e)}^2 + \sum_{e\in\mathcal{E}_h^b} \frac{1}{h} \|v_h - g\|_{L^2(e)}^2. \end{aligned} \tag{2.6}$$

To solve the minimization problem (2.5), one has the corresponding variational equation which takes the following form: find $(u_h, \mathbf{p}_h) \in V_h^m \times \mathbf{W}_h^m$ such that

$$a_h(u_h, \mathbf{p}_h; v_h, \mathbf{q}_h) = l_h(v_h, \mathbf{q}_h) \quad \forall (v_h, \mathbf{q}_h) \in V_h^m \times \mathbf{W}_h^m, \tag{2.7}$$

where the bilinear form $a_h(\cdot;\cdot)$ and the linear form $l_h(\cdot)$ are defined by

$$\begin{aligned} a_h(u_h,\mathbf{p}_h; v_h, \mathbf{q}_h) = & \sum_{K\in\mathcal{T}_h} \left(\int_K \nabla \cdot \mathbf{p}_h \nabla \cdot \mathbf{q}_h \mathrm{d}\boldsymbol{x} + \int_K (\nabla u_h - \mathbf{p}_h)(\nabla v_h - \mathbf{q}_h) \mathrm{d}\boldsymbol{x} \right) \\ & + \sum_{e\in\mathcal{E}_h^i} \int_e \frac{1}{h} [\![u]\!][\![v]\!] \mathrm{d}\boldsymbol{s} + \sum_{e\in\mathcal{E}_h^i} \int_e \frac{1}{h} [\![\mathbf{p}_h]\!][\![\mathbf{q}_h]\!] \mathrm{d}\boldsymbol{s} + \sum_{e\in\mathcal{E}_h^b} \int_e \frac{1}{h} u_h v_h \mathrm{d}\boldsymbol{s} \end{aligned}$$

and

$$l_h(v_h, \mathbf{q}_h) = -\sum_{K\in\mathcal{T}_h}\int_K f\nabla\cdot\mathbf{q}_h \mathrm{d}\boldsymbol{x} + \sum_{e\in\mathcal{E}_h^b}\frac{1}{h}\int_e g v_h \mathrm{d}\boldsymbol{s}.$$

The coercivity of the bilinear form $a_h(\cdot;\cdot)$ is given in [33, Lemma 3.1] as the following.

LEMMA 2.1. *For any $(v_h, \mathbf{q}_h) \in V_h^m \times \mathbf{W}_h^m$, there exists a constant C such that*

$$a_h(v_h, \mathbf{q}_h; v_h, \mathbf{q}_h) \geq C\left(\|v_h\|_u^2 + \|\mathbf{q}_h\|_{\mathbf{p}}^2\right). \tag{2.8}$$

The uniqueness of the solution to (2.7) instantly follows from Lemma 2.1 and the trivial boundedness of $a_h(\cdot;\cdot)$. Further, it is direct to derive the error estimate with respect to the norms $\|\cdot\|_u$ and $\|\cdot\|_{\mathbf{p}}$ by the approximation properties of spaces V_h^m and $\mathbf{W}_h^m$ [33, Theorem 4.1].

THEOREM 2.2. *Let $(u_h, \mathbf{p}_h) \in V_h^m \times \mathbf{W}_h^m$ be the solution to* (2.8)*, and assume the exact solutions $u \in H^{m+1}(\Omega)$ and $\mathbf{p} \in \mathbf{H}^{m+1}(\Omega)$; then there exists a constant C such that*

$$\|u - u_h\|_u + \|\mathbf{p} - \mathbf{p}_h\|_{\mathbf{p}} \leq Ch^m\left(\|u\|_{H^{m+1}(\Omega)} + \|\mathbf{p}\|_{H^{m+1}(\Omega)}\right). \tag{2.9}$$

3. Approximation space with irrotational basis. In this section, we follow the idea in [25, 26] to define an approximation space using a patch reconstruction operator. Purposely, the reconstruction operator we propose here will use the irrotational basis, and thus the approximation space obtained is piecewisely irrotational. With this new approximation space, we will decouple the minimization problem (2.6) into two subproblems: we can numerically solve $\mathbf{p}$ at first and then solve u. Let us first introduce an irrotational polynomial space $\mathbf{S}_m$ which plays a key role in the construction of the operator:

$$\mathbf{S}_m(D) = \left\{\mathbf{v} \in [\mathbb{P}_m(D)]^d \mid \nabla\times\mathbf{v} = 0\right\}.$$

For the irrotational polynomial space, we have the following.

LEMMA 3.1. *For any function $\mathbf{q} \in \mathbf{H}^{m+1}(K) \cap H(\mathrm{curl}^0, K)$, there exists a constant C such that there is a polynomial $\widetilde{\mathbf{q}}_h \in \mathbf{S}_m(K)$ such that*

$$\|\mathbf{q} - \widetilde{\mathbf{q}}_h\|_{L^2(K)} + h_K\|\nabla(\mathbf{q} - \widetilde{\mathbf{q}}_h)\|_{L^2(K)} \leq Ch_K^{m+1}\|\mathbf{q}\|_{H^{m+1}(K)}. \tag{3.1}$$

Proof. Since $H(\mathrm{curl}^0; K) = \nabla H^1(K)$ [20], there exists a $v \in H^{m+2}(K)$ such that $\mathbf{q} = \nabla v$. Let $\widetilde{v} \in \mathbb{P}_{m+2}(K)$ be the standard nodal interpolation polynomial of v, and let $\widetilde{\mathbf{q}}_h = \nabla\widetilde{v}_h$. The inequality (3.1) directly follows from the approximation properties of $\widetilde{v}_h$ [15]. ∎

Let $\mathbf{U}_h$ be the piecewise constant space associated with the partition $\mathcal{T}_h$:

$$\mathbf{U}_h \triangleq \left\{\mathbf{q}_h \in \mathbf{L}^2(\Omega) \mid \mathbf{q}_h|_K \in [\mathbb{P}_0(K)]^d\ \forall K \in \mathcal{T}_h\right\}.$$

We then define a reconstruction operator from $\mathbf{U}_h$ to a piecewisely irrotational polynomial space. For any element $K \in \mathcal{T}_h$, we prescribe a point $\boldsymbol{x}_K \in K$, referred to as the *sampling node* later on, which is preferred to be the barycenter of K. Then, for each element K, we construct an element patch $S(K)$ which is an agglomeration of elements that contain K itself and some elements around K. There are a variety of approaches to building the element patch, and in this paper we agglomerate elements

to form the element patch recursively. For element K, we first let $S_0(K) = \{K\}$ and we define $S_t(K)$ as

$$S_t(K) = S_{t-1}(K) \cup \left\{ K' \mid \exists \widetilde{K} \in S_{t-1}(K) \text{ s.t. } K' \cap \widetilde{K} = e \in \mathcal{E}_h \right\}, \quad t = 1, 2, \ldots.$$

In the implementation of our code, at depth t we enlarge $S_t(K)$ element by element and once $S_t(K)$ has collected a sufficiently large number of elements, we stop the recursive procedure and let $S(K) = S_t(K)$; otherwise, we let $t = t + 1$ and continue the recursion. The cardinality of $S(K)$ is denoted by $\#S(K)$.

Further, for element K we denote by $\mathcal{I}_K$ the set of sampling nodes located inside the element patch $S(K)$:

$$\mathcal{I}_K \triangleq \left\{ \boldsymbol{x}_{\widetilde{K}} \mid \forall \widetilde{K} \in S(K) \right\}.$$

For any piecewise constant function $\mathbf{f} \in \mathbf{U}_h$ and an element $K \in \mathcal{T}_h$, we seek a polynomial $\mathcal{R}_K^m \mathbf{f}$ of degree m defined on $S(K)$ by solving the following least squares problem:

$$\mathcal{R}_K^m \mathbf{f} = \underset{\mathbf{v} \in \mathbf{S}_m(S(K))}{\arg\min} \sum_{\boldsymbol{x}_{\widetilde{K}} \in \mathcal{I}_K} |\mathbf{v}(\boldsymbol{x}_{\widetilde{K}}) - \mathbf{f}(\boldsymbol{x}_{\widetilde{K}})|^2. \tag{3.2}$$

We note that the existence of the solution to (3.2) is obvious but the uniqueness of the solution depends on the position of the sampling nodes in $\mathcal{I}_K$; here we follow [25] to state the following assumption.

ASSUMPTION 1. *For any element $K \in \mathcal{T}_h$ and $\mathbf{v} \in \mathbf{S}_m(S(K))$,*

$$\mathbf{v}|_{\mathcal{I}_K} = \mathbf{0} \quad \textit{implies} \quad \mathbf{v}|_{S(K)} \equiv \mathbf{0}.$$

This assumption demands that the number $\#S(K)$ be greater than $\dim(\mathbf{S}_m)/d$ and excludes the situation that all the points in $\mathcal{I}_K$ lie on an algebraic curve of degree m. Hereafter, we always require that the assumption holds.

Due to the linear dependence of the solution (3.2), a global reconstruction operator $\mathcal{R}^m$ for $\mathbf{f}$ can be defined by restricting the polynomial $\mathcal{R}_K^m \mathbf{f}$ on K:

$$(\mathcal{R}^m \mathbf{f})|_K = (\mathcal{R}_K^m \mathbf{f})|_K \quad \forall K \in \mathcal{T}_h.$$

It is clear that the operator $\mathcal{R}^m$ embeds the piecewise constant space $\mathbf{U}_h$ to a piecewisely irrotational polynomial space of degree m. We denote by $\mathbf{U}_h^m$ the image of the operator $\mathcal{R}^m$. Then we extend the definition domain of the reconstruction operator to the space $\mathbf{C}^0(\Omega) \cap H(\mathrm{curl}^0; \Omega)$. For any $\mathbf{g} \in \mathbf{C}^0(\Omega) \cap H(\mathrm{curl}^0; \Omega)$, we define a piecewise constant function $\widetilde{\mathbf{g}} \in \mathbf{U}_h$ such that

$$\widetilde{\mathbf{g}}(\boldsymbol{x}_K) = \mathbf{g}(\boldsymbol{x}_K) \quad \forall K \in \mathcal{T}_h.$$

We directly set $\mathcal{R}^m \mathbf{g} = \mathcal{R}^m \widetilde{\mathbf{g}}$. Further, we define the function $\mathbf{w}_K^i$ corresponding to the element K as

$$\mathbf{w}_K^i(\boldsymbol{x}) = \begin{cases} \boldsymbol{e}_i, & \boldsymbol{x} = \boldsymbol{x}_K, \\ \mathbf{0}, & \boldsymbol{x} \in \widetilde{K}, \quad \widetilde{K} \neq K, \end{cases} \qquad \forall K \in \mathcal{T}_h,$$

where $\boldsymbol{e}_i$ is a $d \times 1$ unit vector whose ith entry is 1. Then $\mathbf{U}_h^m = \text{span}\{\boldsymbol{\lambda}_K^i \mid \boldsymbol{\lambda}_K^i = \mathcal{R}^m \mathbf{w}_K^i,\ 1 \le i \le d,\ K \in \mathcal{T}_h\}$ and one can write the operator $\mathcal{R}^m$ in an explicit way: for function $\mathbf{g} = (g^1, \ldots, g^d) \in \mathbf{C}^0(\Omega) \cap H(\text{curl}^0; \Omega)$, we have

$$\mathcal{R}^m \mathbf{g} = \sum_{K \in \mathcal{T}_h} \sum_{i=1}^{d} g^i(\boldsymbol{x}_K) \boldsymbol{\lambda}_K^i(\boldsymbol{x}). \tag{3.3}$$

From (3.3), we observe that the DOFs of the operator $\mathcal{R}^m$ are the values of the unknown function at the sampling nodes of all elements in the partition. The number of DOFs is always d times the number of the elements. In Appendix A, we give more details about the computer implementation of our reconstructed space.

We next focus on the approximation property of the operator $\mathcal{R}^m$. For element K, we define a constant

$$\Lambda(m, S(K)) = \max_{v \in \mathbb{P}_m(S(K))} \frac{\max_{\boldsymbol{x} \in S(K)} |v(\boldsymbol{x})|}{\max_{\boldsymbol{x} \in \mathcal{I}_K} |v(\boldsymbol{x})|}.$$

We note that under some mild and practical conditions about $S(K)$, the constant $\Lambda(m, S(K))$ has a uniform upper bound Λ_m, which plays an important role in the approximation property analysis. We refer the reader to [27, 25] for the conditions and more details about the constant $\Lambda(m, S(K))$ and the uniform upper bound. In addition, under such conditions Lemma 3.1 could be generalized as the following.

LEMMA 3.2. *For any function $\mathbf{q} \in \mathbf{H}^{m+1}(S(K)) \cap H(\text{curl}^0, S(K))$, there exists a constant C such that there is a polynomial $\widetilde{\mathbf{q}}_h \in \mathbf{S}_m(S(K))$ such that*

$$\|\mathbf{q} - \widetilde{\mathbf{q}}_h\|_{L^2(S(K))} + h_K \|\nabla (\mathbf{q} - \widetilde{\mathbf{q}}_h)\|_{L^2(S(K))} \le C h_K^{m+1} \|\mathbf{q}\|_{H^{m+1}(S(K))}. \tag{3.4}$$

Proof. It directly follows from [25, Assumption A and Property M3]. ∎

With Λ_m, let us state the approximation property of the operator $\mathcal{R}_K^m$.

THEOREM 3.3. *Let $\mathbf{f} \in \mathbf{H}^{m+1}(\Omega) \cap H(\text{curl}^0; \Omega)$ and $K \in \mathcal{T}_h$; then there exists a constant C such that*

$$\begin{aligned} \|\mathbf{f} - \mathcal{R}_K^m \mathbf{f}\|_{H^q(K)} &\le C \Lambda_m h_K^{m+1-q} \|\mathbf{f}\|_{H^{m+1}(S(K))}, \quad q = 0, 1, \\ \|\nabla^q (\mathbf{f} - \mathcal{R}_K^m \mathbf{f})\|_{L^2(\partial K)} &\le C \Lambda_m h_K^{m+1-q-1/2} \|\mathbf{f}\|_{H^{m+1}(S(K))}, \quad q = 0, 1. \end{aligned} \tag{3.5}$$

Proof. The estimates directly follow the proof of [25, Lemma 2.4] and Lemma 3.2. ∎

4. Sequential least squares finite element approximation. Let us define a new functional $J_h^{\mathbf{P}}(\cdot)$ by

$$\begin{aligned} J_h^{\mathbf{P}}(\mathbf{q}_h) \triangleq \sum_{K \in \mathcal{T}_h} \|\nabla \cdot \mathbf{q}_h + f\|_{L^2(K)}^2 &+ \sum_{e \in \mathcal{E}_h^i} \frac{1}{h} \|[\![\mathbf{q}_h \otimes \mathbf{n}]\!]\|_{L^2(e)}^2 \\ &+ \sum_{e \in \mathcal{E}_h^b} \frac{1}{h} \|\mathbf{q}_h \times \mathbf{n} - \nabla g \times \mathbf{n}\|_{L^2(e)}^2. \end{aligned} \tag{4.1}$$

The terms in $J_h^{\mathbf{P}}(\mathbf{q}_h)$ include the part related to the flux in (2.6) and the term on the boundary. We minimize this functional in $\mathbf{U}_h^m$ to have an approximating flux. The corresponding minimization problem reads as follows: find $\mathbf{p}_h \in \mathbf{U}_h^m$ such that

$$J_h^{\mathbf{P}}(\mathbf{p}_h) = \inf_{\mathbf{q}_h \in \mathbf{U}_h^m} J_h^{\mathbf{P}}(\mathbf{q}_h). \tag{4.2}$$

The Euler–Lagrange equation of this minimization problem is as follows: find $\mathbf{p}_h \in \mathbf{U}_h^m$ such that

$$a_h^{\mathbf{P}}(\mathbf{p}_h, \mathbf{q}_h) = l_h^{\mathbf{P}}(\mathbf{q}_h) \quad \forall \mathbf{q}_h \in \mathbf{U}_h^m, \tag{4.3}$$

where the bilinear form $a_h^{\mathbf{P}}(\cdot,\cdot)$ is

$$a_h^{\mathbf{P}}(\mathbf{p}_h, \mathbf{q}_h) = \sum_{K\in\mathcal{T}_h} \int_K (\nabla\cdot\mathbf{p}_h)(\nabla\cdot\mathbf{q}_h)\mathrm{d}\boldsymbol{x} + \sum_{e\in\mathcal{E}_h^i} \int_e \frac{1}{h}[\![\mathbf{p}_h\otimes\mathbf{n}]\!][\![\mathbf{q}_h\otimes\mathbf{n}]\!]\mathrm{d}\boldsymbol{s} + \sum_{e\in\mathcal{E}_h^b} \int_e \frac{1}{h}(\mathbf{p}_h\times\mathbf{n})\cdot(\mathbf{q}_h\times\mathbf{n})\mathrm{d}\boldsymbol{s},$$

and the linear form $l_h^{\mathbf{P}}(\cdot)$ is

$$l_h^{\mathbf{P}}(\mathbf{q}_h) = -\sum_{K\in\mathcal{T}_h} \int_K f\nabla\cdot\mathbf{q}_h\mathrm{d}\boldsymbol{x} + \sum_{e\in\mathcal{E}_h^b} \int_e \frac{1}{h}(\mathbf{p}_h\times\mathbf{n})\cdot(\nabla g\times\mathbf{n})\mathrm{d}\boldsymbol{s}.$$

Let

$$|\!|\!|\mathbf{q}_h|\!|\!|_{\mathbf{P}}^2 \triangleq \sum_{K\in\mathcal{T}_h} \|\nabla\cdot\mathbf{q}_h\|_{L^2(K)}^2 + \sum_{e\in\mathcal{E}_h^i} \frac{1}{h}\|[\![\mathbf{q}_h\otimes\mathbf{n}]\!]\|_{L^2(e)}^2 + \sum_{e\in\mathcal{E}_h^b} \frac{1}{h}\|\mathbf{q}_h\times\mathbf{n}\|_{L^2(e)}^2 \tag{4.4}$$

$\forall\mathbf{q}_h \in \mathbf{U}_h^m + \mathbf{H}^1(\Omega)\cap H(\mathrm{curl}^0;\Omega)$. The following lemma shows that $|\!|\!|\cdot|\!|\!|_{\mathbf{P}}$ actually defines a norm on the space $\mathbf{U}_h^m + \mathbf{H}^1(\Omega)\cap H(\mathrm{curl}^0;\Omega)$, referred to as the *energy norm* later on.

LEMMA 4.1. *For any* $\mathbf{q}_h \in \mathbf{U}_h^m + \mathbf{H}^1(\Omega)\cap H(\mathrm{curl}^0;\Omega)$*, there exists a constant* C *such that*

$$\|\mathbf{q}_h\|_{L^2(\Omega)} \le C|\!|\!|\mathbf{q}_h|\!|\!|_{\mathbf{P}}. \tag{4.5}$$

Proof. The idea follows [7, Lemma 1] to apply the orthogonal decomposition of $\mathbf{L}^2(\Omega)$. We only prove for the case $d = 2$, and it is almost trivial to extend the result for three-dimensional case. Since $\mathbf{q}_h \in \mathbf{L}^2(\Omega)$, we let $\phi \in H^1(\Omega)\backslash\mathbb{R}$ be the only solution of

$$(\nabla\times\phi, \nabla\times\chi) = (\mathbf{q}_h, \nabla\times\chi) \quad \forall\chi \in H^1(\Omega).$$

This solution ϕ satisfies

$$-\Delta\phi = \nabla\times\mathbf{q}_{\mathbf{h}} \quad \text{in } H^{-1}(\Omega).$$

Applying Green's formula, we have

$$0 = (\mathbf{q}_h - \nabla\times\phi, \nabla\times\chi) = ((\mathbf{q}_h - \nabla\times\phi)\times\mathbf{n}, \chi)_{L^2(\partial\Omega)} \quad \forall\chi \in H^1(\Omega).$$

Thus there exists $v \in H_0^1(\Omega)$ such that $\nabla v = \mathbf{q}_h - \nabla\times\phi$ [20]. In addition, we have the stability estimates

$$\|\phi\|_{H^1(\Omega)} \le C\|\mathbf{q}_h\|_{L^2(\Omega)}, \quad \|v\|_{H^1(\Omega)} \le C\|\mathbf{q}_h\|_{L^2(\Omega)}. \tag{4.6}$$

Further, we use the decomposition to obtain

$$\begin{aligned}\|\mathbf{q}_h\|^2_{L^2(\Omega)} &= \left(\sum_{K\in\mathcal{T}_h}\int_K \mathbf{q}_h\cdot\nabla v\mathrm{d}\boldsymbol{x} + \int_K \mathbf{q}_h\cdot\nabla\times\chi\mathrm{d}\boldsymbol{x}\right)\\ &= \sum_{K\in\mathcal{T}_h}\left(\int_{\partial K} v\mathbf{q}_h\cdot\mathbf{n}\mathrm{d}\boldsymbol{s} - \int_K v\nabla\cdot\mathbf{q}_h\mathrm{d}\boldsymbol{x} + \int_{\partial K}\chi\mathbf{q}_h\times\mathbf{n}\mathrm{d}\boldsymbol{s}\right)\\ &= \sum_{e\in\mathcal{E}_h^i}\int_e (v[\![\mathbf{q}_h\cdot\mathbf{n}]\!] + \chi[\![\mathbf{q}_h\times\mathbf{n}]\!])\,\mathrm{d}\boldsymbol{s} + \sum_{e\in\mathcal{E}_h^b}\int_e \chi\mathbf{q}_h\times\mathbf{n}\mathrm{d}\boldsymbol{s} - \int_K v\nabla\cdot\mathbf{q}_h\mathrm{d}\boldsymbol{x}.\end{aligned}$$

And we have that

$$\sum_{e\in\mathcal{E}_h^i}\int_e \left(\|[\![\mathbf{q}_h\cdot\mathbf{n}]\!]\|^2_{L^2(e)} + \|[\![\mathbf{q}_h\times\mathbf{n}]\!]\|^2_{L^2(e)}\right)\mathrm{d}\boldsymbol{s} \le C\sum_{e\in\mathcal{E}_h^i}\int_e \|[\![\mathbf{q}_h\otimes\mathbf{n}]\!]\|^2_{L^2(e)}\mathrm{d}\boldsymbol{s}.$$

Using the Cauchy–Schwarz inequality, trace inequality (2.1), and the stability estimate (4.6) could yield the estimate (4.5), which completes the proof. ∎

Since $\forall\mathbf{q}_h\in\mathbf{U}_h^m+\mathbf{H}^1(\Omega)\cap H(\mathrm{curl}^0;\Omega)$ we have $a_h^{\mathbf{P}}(\mathbf{q}_h,\mathbf{q}_h)=|\!|\!|\mathbf{q}_h|\!|\!|^2_{\mathbf{p}}$, it is implied that the problem (4.3) has a unique solution. Moreover, we could establish the convergence result with respect to the norm $|\!|\!|\cdot|\!|\!|_{\mathbf{p}}$.

THEOREM 4.2. *Let* $\mathbf{p}\in\mathbf{H}^{m+1}(\Omega)\cap H(\mathrm{curl}^0;\Omega)$ *be the exact solution, and let* $\mathbf{p}_h\in\mathbf{U}_h^m$ *be the solution to* (4.3)*; then we have*

$$|\!|\!|\mathbf{p}-\mathbf{p}_h|\!|\!|_{\mathbf{p}} \le Ch^m\|\mathbf{p}\|_{H^{m+1}(\Omega)}. \tag{4.7}$$

Proof. Since $\mathbf{p}_h$ minimizes the problem (4.2) and $[\![\mathbf{p}\otimes\mathbf{n}]\!]=0$, we have

$$|\!|\!|\mathbf{p}-\mathbf{p}_h|\!|\!|^2_{\mathbf{p}} = J_h^{\mathbf{p}}(\mathbf{p}_h) \le J_h^{\mathbf{p}}(\mathcal{R}^m\mathbf{p}) = |\!|\!|\mathbf{p}-\mathcal{R}^m\mathbf{p}|\!|\!|^2_{\mathbf{p}}.$$

Therefore, we only need to bound $|\!|\!|\mathbf{p}-\mathcal{R}^m\mathbf{p}|\!|\!|_{\mathbf{p}}$.

By the approximation (3.5) and trace inequality (2.1), we obtain that for element K,

$$\|\nabla\cdot\mathbf{p}-\nabla\cdot\mathcal{R}^m\mathbf{p}\|_{L^2(K)} \le Ch_K^m\|\mathbf{p}\|_{H^{m+1}(S(K))},$$

and

$$\begin{aligned}\|(\mathbf{p}-\mathcal{R}^m\mathbf{p})\otimes\mathbf{n}\|^2_{L^2(\partial K)} &\le C\|\mathbf{p}-\mathcal{R}^m\mathbf{p}\|^2_{L^2(\partial K)}\\ &\le C(h_K^{-1}\|\mathbf{p}-\mathcal{R}^m\mathbf{p}\|^2_{L^2(K)} + h_K\|\nabla(\mathbf{p}-\mathcal{R}^m\mathbf{p})\|^2_{L^2(K)})\\ &\le Ch_K^{2m+1}\|\mathbf{p}\|^2_{H^{m+1}(S(K))}.\end{aligned}$$

The inequality (4.7) is concluded by summing over all elements in the partition, which completes the proof. ∎

Remark 1. From the estimates (4.5) and (4.7) we can only prove a suboptimal convergence rate of $\|\mathbf{p}-\mathbf{p}_h\|_{L^2(\Omega)}$. The numerical results in section 5 reveal the optimal L^2 convergence rate for odd m and the suboptimal rate for even m. This odd/even situation has also been detected in some DG methods, such as the IIPG method or the NIPG method, and it is still an open problem. We refer the reader to [23, 17, 4] and the references therein for more discussion about L^2 optimality.

After getting the numerical flux $\mathbf{p}_h$, the next step is to plug it into the functional (2.6) to calculate the pressure u. We define the functional $J_h^u(\cdot)$ as follows:

$$J_h^u(v) \triangleq \sum_{K\in\mathcal{T}_h} \|\nabla v - \mathbf{p}_h\|_{L^2(K)}^2 + \sum_{e\in\mathcal{E}_h^i} \frac{1}{h}\|[\![v]\!]\|_{L^2(e)}^2 + \sum_{e\in\mathcal{E}_h^b} \frac{1}{h}\|v-g\|_{L^2(e)}^2. \tag{4.8}$$

To get an approximation to u, one may solve the minimization problem for the functional $J_h^u(\cdot)$ in a certain approximation space. We note that it is very flexible to choose the approximation space for u. For instance, one may use the discontinuous finite element space V_h^m or the patch reconstructed space proposed in [25]. Here we solve the pressure u with the standard Lagrange finite element space, which is defined as

$$\widehat{V}_h^m \triangleq \{v_h \in C(\Omega) \mid v_h|_K \in \mathbb{P}_m(K)\ \forall K \in \mathcal{T}_h\}.$$

Due to the continuity of the space $\widehat{V}_h^m$, the functional $J_h^u(v)$ is simplified as

$$J_h^u(v) = \sum_{K\in\mathcal{T}_h} \|\nabla v - \mathbf{p}_h\|_{L^2(K)}^2 + \sum_{e\in\mathcal{E}_h^b} \frac{1}{h}\|v-g\|_{L^2(e)}^2 \quad \forall v \in H^1(\Omega). \tag{4.9}$$

The following minimization problem gives the numerical solution to the pressure u in $\widehat{V}_h^m$:

$$\min_{v_h\in\widehat{V}_h^m} J_h^u(v_h).$$

The discrete variational problem equivalent to the minimization problem reads as follows: find $u_h \in \widehat{V}_h^m$ such that

$$a_h^u(u_h, v_h) = l_h^u(v_h) \quad \forall v_h \in \widehat{V}_h^m, \tag{4.10}$$

where the bilinear form $a_h^u(\cdot,\cdot)$ is given by

$$a_h^u(u_h, v_h) = \sum_{K\in\mathcal{T}_h} \int_K \nabla u_h \cdot \nabla v_h \mathrm{d}\boldsymbol{x} + \sum_{e\in\mathcal{E}_h^b} \int_e \frac{1}{h} u_h v_h \mathrm{d}\boldsymbol{s},$$

and the linear form $l_h^u(\cdot)$ is given by

$$l_h^u = \sum_{K\in\mathcal{T}_h} \int_K \nabla v_h \cdot \mathbf{p}_h \mathrm{d}\boldsymbol{x} + \sum_{e\in\mathcal{E}_h^b} \int_e \frac{1}{h} v_h g \mathrm{d}\boldsymbol{s}.$$

Analogous to the procedure we use to solve the flux $\mathbf{p}$, we define $|\!|\!| \cdot |\!|\!|_u$ as

$$|\!|\!| v |\!|\!|_u^2 \triangleq \sum_{K\in\mathcal{T}_h} \|\nabla v\|_{L^2(K)}^2 + \sum_{e\in\mathcal{E}_h^b} \frac{1}{h}\|v\|_{L^2(e)}^2 \quad \forall v \in H^1(\Omega).$$

The inequality $\|v\|_{L^2(\Omega)} \le C|\!|\!|v|\!|\!|_u$ [2, Lemma 2.1] ensures that $|\!|\!| \cdot |\!|\!|_u$ is actually a norm on $H^1(\Omega)$, which actually guarantees the unisolvability of the problem (4.10). $|\!|\!| \cdot |\!|\!|_u$ is referred as the *energy norm* on $\widehat{V}_h^m$ from now on. Further, the error estimate with respect to $|\!|\!| \cdot |\!|\!|_u$ is given in the theorem below as follows.

THEOREM 4.3. *Let $u \in H^{m+1}(\Omega)$ be the exact solution, and let $u_h \in \widehat{V}_h^m$ be the solution to* (4.10)*; then we have*

$$|\!|\!| u - u_h |\!|\!|_u \le C\|\mathbf{p} - \mathbf{p}_h\|_{L^2(\Omega)} + Ch^m \|u\|_{H^{m+1}(\Omega)}, \tag{4.11}$$

where $\mathbf{p}_h$ is the solution to (4.2).

Proof. Let $u_I \in \widehat{V}_h^m$ be the interpolant of u, and we have that

$$\begin{aligned} J_h^u(u_h) &\le J_h^u(u_I), \\ |\!|\!| u - u_h |\!|\!|_u^2 &\le C(J_h^u(u_I) + \|\nabla u - \mathbf{p}_h\|_{L^2(\Omega)}^2) \\ &\le C\left(|\!|\!| u - u_I |\!|\!|_u^2 + \|\mathbf{p} - \mathbf{p}_h\|_{L^2(\Omega)}^2 \right). \end{aligned}$$

The approximation property of the space $\widehat{V}_h^m$ [15] gives us

$$|\!|\!| u - u_I |\!|\!|_u \le C h^m \|u\|_{H^{m+1}(\Omega)},$$

which yields the estimate (4.11) and completes the proof. ∎

Then we can have the error estimate under the L^2 norm.

THEOREM 4.4. *Let $u \in H^{m+1}(\Omega)$ be a solution, and let $u_h \in \widehat{V}_h^m$ be the solution to* (4.10)*; then we have*

$$\|u - u_h\|_{L^2(\Omega)} \le C_0 \|\mathbf{p} - \mathbf{p}_h\|_{L^2(\Omega)} + C_1 h^{m+1} \|u\|_{H^{m+1}(\Omega)}, \tag{4.12}$$

where $\mathbf{p}_h$ is the solution to (4.2).

Proof. Let $e_h = u - u_h$, and from the definition of $a_h^u(\cdot,\cdot)$, one sees that

$$a_h^u(e_h, v_h) = (\mathbf{p} - \mathbf{p}_h, v_h) \quad \forall v_h \in \widehat{V}_h^m.$$

We first show that $\|e_h\|_{H^{-1/2}(\partial\Omega)} \le C_0 h |\!|\!| e_h |\!|\!|_u + C_1 h \|\mathbf{p} - \mathbf{p}_h\|_{L^2(\Omega)}$, where

$$\|e_h\|_{H^{-1/2}(\partial\Omega)} = \sup_{\tau \in H^{1/2}(\partial\Omega)} \frac{(e_h, \tau)_{L^2(\partial\Omega)}}{\|\tau\|_{H^{1/2}(\partial\Omega)}}.$$

We let $\alpha \in H^1(\Omega)$, which solves $\Delta\alpha = 0$ in Ω and $\alpha = \tau$ on $\partial\Omega$, and we let $\alpha_I \in \widehat{V}_h^m$ be the interpolant of α. Then we have that

$$\begin{aligned} (e_h, \tau)_{L^2(\partial\Omega)} &= h(h^{-1}(e_h, \alpha)_{L^2(\partial\Omega)}) \\ &= h(h^{-1}(e_h, \alpha)_{L^2(\partial\Omega)} - a_h^u(e_h, \alpha_I)) + h(\mathbf{p} - \mathbf{p}_h, \alpha_I) \\ &= h(h^{-1}(e_h, \alpha - \alpha_I)_{L^2(\partial\Omega)} - (\nabla e_h, \nabla \alpha_I)_{L^2(\Omega)}) + h(\mathbf{p} - \mathbf{p}_h, \alpha_I) \\ &\le C_0 h |\!|\!| e_h |\!|\!|_u (\|h(\alpha - \alpha_I)\|_{L^2(\partial\Omega)} + \|\nabla \alpha_I\|_{L^2(\Omega)}) + C_1 h \|\mathbf{p} - \mathbf{p}_h\|_{L^2(\Omega)} \|\alpha_I\|_{L^2(\Omega)} \\ &\le C_0 h |\!|\!| u_h |\!|\!|_u \|\alpha\|_{H^1(\Omega)} + C_1 h \|\mathbf{p} - \mathbf{p}_h\|_{L^2(\Omega)} \|\alpha\|_{H^1(\Omega)}. \end{aligned}$$

We complete the proof by the regularity estimate $\|\alpha\|_{H^1(\Omega)} \le C\|\tau\|_{H^{1/2}(\partial\Omega)}$.

Given $\psi \in L^2(\Omega)$, we let $w \in H^2(\Omega)$, which solves $-\Delta w = \psi$ in Ω and $w = 0$ on $\partial\Omega$. We denote by $w_I \in \widehat{V}_h^m$ the interpolant of w. Then we could deduce that

$$\begin{aligned} (e_h, \psi) &= (\nabla e_h, \nabla w) - \left(e_h, \frac{\partial w}{\partial \mathbf{n}} \right)_{L^2(\partial\Omega)} \\ &= a_h^u(e_h, w - w_I) + (\mathbf{p} - \mathbf{p}_h, w_I) - \left(e_h, \frac{\partial w}{\partial \mathbf{n}} \right)_{L^2(\partial\Omega)} \\ &\le C h |\!|\!| e_h |\!|\!| \|w\|_{H^2(\Omega)} + \|\mathbf{p} - \mathbf{p}_h\|_{L^2(\Omega)} \|w\|_{H^2(\Omega)} + \|e_h\|_{H^{-1/2}(\partial\Omega)} \left\| \frac{\partial w}{\partial \mathbf{n}} \right\|_{H^{1/2}(\partial\Omega)}. \end{aligned}$$

Let $\psi = e_h$, and combining the bound of $\|e_h\|_{H^{-1/2}(\Omega)}$, the regularity estimate $\|w\|_{H^2(\Omega)} \le C\|\psi\|_{L^2(\Omega)}$, and the approximation property of $|\!|\!| e_h |\!|\!|_u$ could yield the estimate (4.12), which completes the proof. ∎

TABLE 1
$\#S(K)$ *for* $1 \le m \le 3$.

$d = 2$	m	1	2	3
	$\#S(K)$	6	10	16
$d = 3$	m	1	2	3
	$\#S(K)$	8	15	25

Remark 2. Until now the method we established is only for the problem with the Dirichlet boundary condition. For the Neumann boundary condition $\nabla u \cdot \mathbf{n} = g$ on $\partial\Omega$, the boundary term in (4.1) and (4.9) should be modified as

$$\sum_{e\in\mathcal{E}_h^b} \frac{1}{h}\|\mathbf{q}_h \cdot \mathbf{n} - g\|^2_{L^2(e)} \qquad \text{and} \qquad \sum_{e\in\mathcal{E}_h^b} \frac{1}{h}\left\|\frac{\partial v}{\partial \mathbf{n}} - g\right\|^2_{L^2(e)},$$

respectively. It is almost trivial to extend our method in this section to the problem with the Neumann boundary condition.

5. Numerical results. In this section, we conduct some numerical experiments to show the accuracy and efficiency of the proposed method in section 4. For simplicity, we select the cardinality $\#S(K)$ uniformly and we list a group of reference values of $\#S(K)$ for different m in Table 1.

5.1. Convergence order study. We first examine the numerical convergence to verify the theoretical prediction and exhibit the flexibility of our method.

Example 1. We first consider a two-dimensional Poisson problem with a Dirichlet boundary condition on the domain $\Omega = [0, 1] \times [0, 1]$. The exact solution $u(x, y)$ is taken as

$$u(x, y) = \sin(2\pi x)\sin(4\pi y),$$

and the source term f and the boundary data g are chosen accordingly.

We solve this problem on a series of triangular meshes (see Figure 1) with mesh sizes $h = 1/10, 1/20, \ldots, 1/160$, and we first use the space pairs $\mathbf{U}_h^m \times \widehat{V}_h^m (1 \le m \le 3)$ to solve the flux and pressure. In this setting, from (4.12) we could see that the optimal convergence order of u_h depends on the convergence rate of $\|\mathbf{p} - \mathbf{p}_h\|_{L^2(\Omega)}$. Although we cannot develop a theoretical verification for the optimal convergence of $\mathbf{p}_h$ under the L^2 norm, the computed convergence rates of $\|\mathbf{p} - \mathbf{p}_h\|_{L^2(\Omega)}$ seem optimal for odd m. The L^2 norm and the energy norm of the errors in the approximation to the exact solution are gathered in Table 2. We could observe that for odd m, the errors $\|u - u_h\|_{L^2(\Omega)}$, $|||u - u_h|||_u$, $\|\mathbf{p} - \mathbf{p}_h\|_{L^2(\Omega)}$, and $|||\mathbf{p} - \mathbf{p}_h|||_{\mathbf{p}}$ converge to zero optimally as the mesh is refined. For even m, the orders of convergence under the L^2 norm are suboptimal. Moreover, from the estimate (4.12) one could observe that if we decrease the space approximating pressure by one order, we could obtain the optimality for u approximations. The errors with the space pairs $\mathbf{U}_h^m \times \widehat{V}_h^{m-1}$ are collected in Table 3, which clearly shows the optimal convergence of u_h for both measurements. In addition, we note that all the convergence rates are consistent with the theoretical predictions.

Example 2. In this example, we consider the sample problem as in Example 1. But we use a sequence of polygonal meshes consisting of elements with various geometries (see Figure 2), which are generated by `PolyMesher` [32]. We only solve the flux, and we present the corresponding errors in the energy norm and L^2 norm and

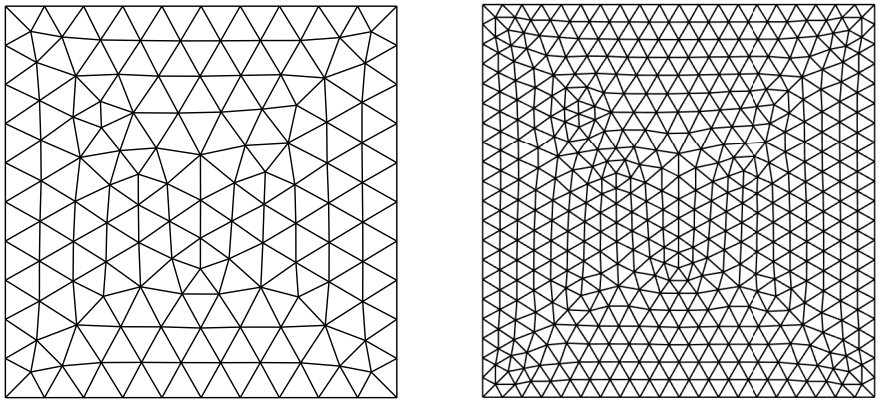

FIG. 1. *The triangular meshes with mesh size* $h = 1/10$ *(left) and* $h = 1/20$ *for Example* 1.

TABLE 2

Example 1. *The errors* $e_u = u - u_h$, $e_{\mathbf{p}} = \mathbf{p} - \mathbf{p}_h$, *and the orders of convergence with the spaces* $\mathbf{U}_h^m \times \widehat{V}_h^m (1 \le m \le 3)$.

m		$\|e_u\|_{L^2(\Omega)}$	Order	$\|\|\|e_u\|\|\|_u$	Order	$\|e_{\mathbf{p}}\|_{L^2(\Omega)}$	Order	$\|\|\|e_{\mathbf{p}}\|\|\|_{\mathbf{p}}$	Order
1	1	1.0602e-01	-	2.5550e-00	-	1.1553e-00	-	2.9109e+01	-
	2	3.0872e-02	1.80	1.2677e-00	1.01	3.3347e-01	1.80	1.5319e+01	0.93
	3	8.3590e-03	1.90	6.3053e-01	1.01	8.7712e-02	1.90	7.9176e+00	0.95
	4	2.1548e-03	1.96	3.1463e-01	1.00	2.2647e-02	1.96	4.0133e+00	0.98
	5	5.4473e-04	1.98	1.5723e-02	1.00	5.7033e-03	1.98	2.0137e+00	1.00
2	1	5.5862e-02	-	9.3425e-01	-	9.1461e-01	-	8.0168e+00	-
	2	1.8898e-02	1.57	2.8628e-01	1.71	2.7402e-01	1.73	1.7807e+00	2.17
	3	4.9746e-03	1.93	7.3469e-02	1.93	7.1190e-02	1.95	4.1888e-01	2.08
	4	1.2538e-03	1.99	1.8776e-02	1.98	1.8016e-02	1.98	1.0111e-01	2.03
	5	3.1393e-04	2.00	4.7137e-03	1.99	4.5126e-03	2.00	2.4633e-02	2.02
3	1	5.2485e-03	-	1.6872e-01	-	1.2492e-01	-	3.7196e+00	-
	2	3.9516e-04	3.73	1.9952e-02	3.07	9.2700e-03	3.75	4.6565e-01	2.95
	3	2.1869e-05	4.17	2.0437e-03	3.28	5.9833e-04	3.95	6.0447e-02	2.97
	4	1.1300e-06	4.27	2.2652e-04	3.17	3.8808e-05	3.95	7.7175e-03	2.97
	5	6.0716e-08	4.07	2.7352e-05	3.05	2.4584e-06	3.98	9.7343e-04	2.99

their respective computed rates in Table 4. Again we observe the optimal convergence for both norms when m is odd. For even m, $\|\mathbf{p}-\mathbf{p}_h\|_{L^2(\Omega)}$ tends to zero in a suboptimal way. To apply the method on meshes with different geometry, it is an advantage inherited from the DG method. On such meshes, the convergence order agrees with our error estimates again.

Example 3. In this example, we consider the mild wave front problem, which is the Poisson equation on the unit square with Dirichlet boundary conditions. The data functions f and g are selected such that the exact solution is

$$u(x, y) = \arctan(\alpha(r - r_0)), \quad (x, y) \in [0, 1]^2,$$

where $r = \sqrt{(x - x_0)^2 + (y - y_0)^2}$. The mild wave front uses $(x_0, y_0) = (-0.05, -0.05)$, $r_0 = 0.7$, and $\alpha = 10$, and it is a problem of near singularities. For this problem, the high-order accuracy is preferred [29]. We use a sequence of quasi-uniform triangular meshes (see Figure 3), and we solve the problem with spaces $\mathbf{U}_h^m \times \widehat{V}_h^m (1 \le m \le 3)$. We list the errors in approximation to $\mathbf{p}$ and u in Table 5. It is clear that the proposed method yields the same convergence rates as Example 1, which validates our

TABLE 3
Example 1. *The errors* $e_u = u - u_h$, $e_{\mathbf{p}} = \mathbf{p} - \mathbf{p}_h$, *and the orders of convergence with the spaces* $\mathbf{U}_h^m \times \widehat{V}_h^{m-1} (2 \le m \le 3)$.

m		$\|e_u\|_{L^2(\Omega)}$	Order	$\|\!\|\!\|e_u\|\!\|\!\|_u$	Order	$\|e_{\mathbf{p}}\|_{L^2(\Omega)}$	Order	$\|\!\|\!\|e_{\mathbf{p}}\|\!\|\!\|_{\mathbf{p}}$	Order
	1	6.8296e-02	-	2.4561e-00	-	9.1461e-01	-	8.0168e+00	-
	2	1.7533e-02	1.96	1.2484e-00	0.97	2.7402e-01	1.73	1.7807e+00	2.17
2	3	4.4126e-03	1.99	6.2683e-01	0.99	7.1190e-02	1.95	4.1888e-01	2.08
	4	1.1050e-03	2.00	3.3137e-01	1.00	1.8016e-02	1.98	1.0111e-01	2.03
	5	2.7636e-04	2.00	1.5691e-01	1.00	4.5126e-03	2.00	2.4633e-02	2.02
	1	4.9662e-03	-	3.8263e-01	-	1.2492e-01	-	3.7196e+00	-
	2	6.3248e-04	2.97	9.7317e-02	1.97	9.2700e-03	3.75	4.6565e-01	2.95
3	3	7.9437e-05	2.99	2.4434e-02	1.99	5.9833e-04	3.95	6.0447e-02	2.97
	4	9.9415e-06	3.00	6.1151e-03	2.00	3.8808e-05	3.95	7.7175e-03	2.97
	5	1.2430e-06	3.00	1.5291e-03	2.00	2.4584e-06	3.98	9.7343e-04	2.99

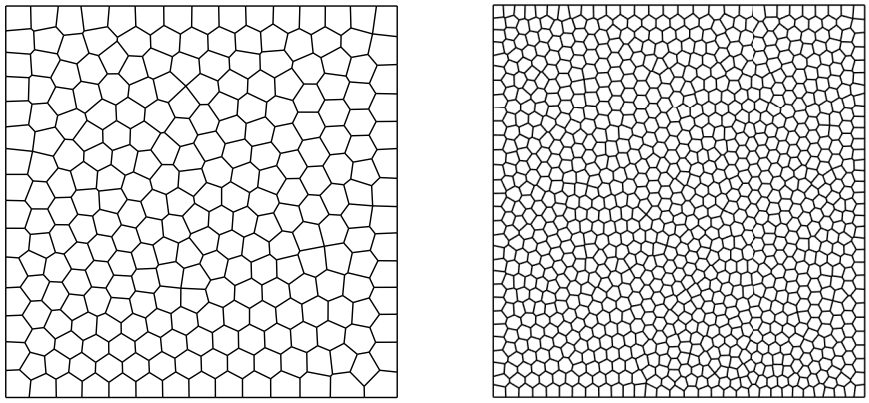

FIG. 2. *The polygonal meshes with* 250 *elements (left)/*1000 *elements (right).*

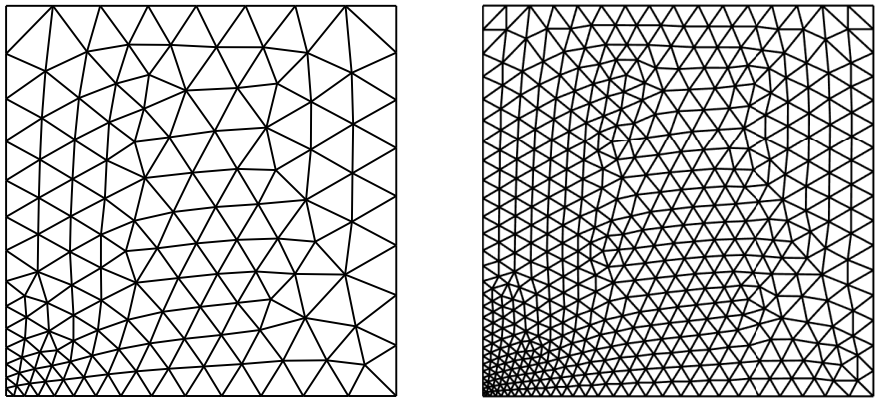

FIG. 3. *The triangular meshes with* 246 *elements (left) and* 984 *elements (right) for Example* 3.

theoretical estimates.

Example 4. In this example, we exhibit the performance of the proposed method with the problem with a corner singularity. We consider the L-shaped domain $\Omega = [-1,1]^2 \backslash [0,1) \times (-1,0]$, and we use a series of triangular meshes; see Figure 4. Fol-

TABLE 4

Example 2. *The errors* $e_{\mathbf{p}} = \mathbf{p} - \mathbf{p}_h$ *and the orders of convergence with the spaces* $\mathbf{U}_h^m (1 \leq m \leq 3)$.

m	DOFs	$\|e_{\mathbf{p}}\|_{L^2(\Omega)}$	Order	$\|e_{\mathbf{p}}\|_{\mathbf{p}}$	Order
1	500	1.0485e-00	-	2.6456e+01	-
	2000	2.7316e-01	1.94	1.3244e+01	0.99
	8000	6.5948e-02	2.05	6.5998e-00	1.00
	32000	1.6203e-02	2.03	3.2658e-00	1.01
2	500	4.4773e-01	-	6.1493e-00	-
	2000	1.2630e-01	1.83	1.3713e-00	2.16
	8000	3.0209e-02	2.06	3.3353e-01	2.03
	32000	7.4860e-03	2.01	8.2873e-02	2.01
3	500	1.6412e-01	-	4.5508e-00	-
	2000	1.0449e-02	3.97	6.2226e-01	2.88
	8000	6.3315e-04	4.05	8.1210e-02	2.95
	32000	3.8188e-05	4.03	1.0205e-02	2.99

TABLE 5

Example 3. *The errors* $e_u = u - u_h$, $e_{\mathbf{p}} = \mathbf{p} - \mathbf{p}_h$, *and the orders of convergence with the spaces* $\mathbf{U}_h^m \times \widehat{V}_h^m (1 \leq m \leq 3)$.

m		$\|e_u\|_{L^2(\Omega)}$	Order	$\|\|\|e_u\|\|\|_u$	Order	$\|e_{\mathbf{p}}\|_{L^2(\Omega)}$	Order	$\|\|\|e_{\mathbf{p}}\|\|\|_{\mathbf{p}}$	Order
1	1	4.3807e-02	-	4.9822e-01	-	1.1553e-00	-	1.0256e+01	-
	2	1.6473e-02	1.41	4.0917e-01	1.03	3.3347e-01	1.80	5.3347e+00	0.95
	3	3.5661e-03	2.21	1.9515e-01	1.07	8.7712e-02	1.90	2.6486e+00	1.01
	4	8.6682e-04	2.03	9.5962e-02	1.02	2.2647e-02	1.96	1.3231e+00	1.00
	5	2.1263e-04	2.03	4.7761e-02	1.00	5.7033e-03	1.98	6.6057e-01	1.00
2	1	1.5200e-02	-	2.9032e-01	-	2.4411e-01	-	5.6918e+00	-
	2	5.3703e-03	1.51	9.0132e-02	1.68	8.9263e-02	1.45	1.3870e+00	2.03
	3	1.4510e-03	1.89	2.5011e-02	1.85	2.5413e-02	1.82	3.1295e-01	2.10
	4	3.6778e-04	1.98	6.5013e-02	2.00	6.7113e-03	1.92	7.1999e-02	2.11
	5	9.1211e-05	2.01	1.6380e-03	1.98	1.6989e-03	1.99	1.7550e-02	2.03
3	1	1.0333e-02	-	8.0091e-02	-	2.0391e-01	-	5.8500e+00	-
	2	1.1023e-03	3.23	1.2076e-02	2.72	1.7701e-02	3.52	9.7265e-01	2.59
	3	6.7612e-05	4.03	1.2368e-03	3.28	1.1398e-03	3.96	1.3999e-01	2.80
	4	4.2528e-06	4.00	1.2956e-04	3.26	7.4761e-05	3.93	1.8073e-02	2.96
	5	2.2322e-07	4.12	1.4319e-05	3.17	4.7259e-06	3.98	2.2425e-03	3.01

lowing [28], we let the exact solution be

$$u(r, \theta) = r^{5/3} \sin(5\theta/3)$$

in the polar coordinate and impose the Dirichlet boundary condition. The data f and the function g are chosen accordingly. We notice that $u(r, \theta)$ only belongs to H^{2+s} with $s < 2/3$. In Table 6, we list the errors measured in the energy norm and L^2 norm for both flux and pressure. Here we observe that the error $\|\|\mathbf{p} - \mathbf{p}_h\|\|_{\mathbf{p}}$ decreases at the rate $O(h^{2/3})$, which matches with the fact that $\mathbf{p}$ only belongs to $H^{5/3-\varepsilon}(\Omega)$. The computed orders of $\|\mathbf{p} - \mathbf{p}_h\|_{L^2(\Omega)}$, $\|\|u - u_h\|\|_u$ and $\|u - u_h\|_{L^2(\Omega)}$ are about 1. A possible explanation of the rates may be traced back to the lack of H^3-regularity of the exact solution on the whole domain.

Example 5. We consider a three-dimensional Poisson problem on a unit cube $\Omega = [0, 1]^3$. The domain is partitioned into a series of tetrahedral meshes with mesh sizes $h = 1/5, 1/10, 1/20, 1/40$ by `Gmsh` [19]. The exact solution is taken as

$$u(x, y, z) = \sin(2\pi x) \sin(2\pi y) \sin(2\pi z),$$

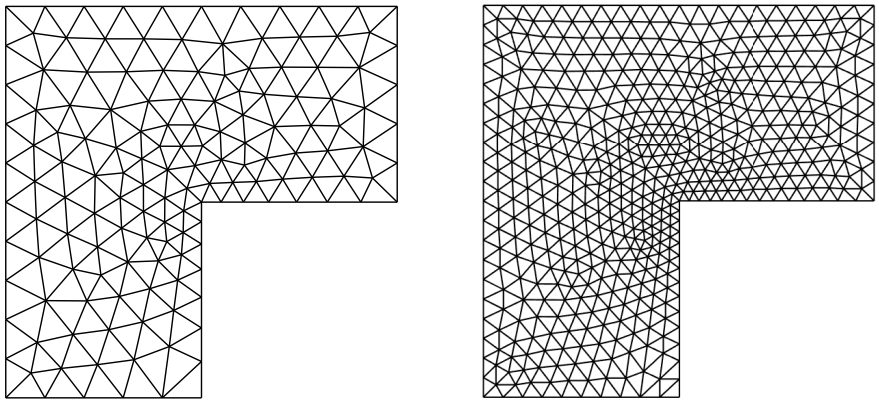

FIG. 4. *The triangular meshes with* 250 *elements (left) and* 1000 *elements for Example* 3.

TABLE 6

Example 4. *The errors* $e_u = u - u_h$, $e_{\mathbf{p}} = \mathbf{p} - \mathbf{p}_h$, *and the orders of convergence with the spaces* $\mathbf{U}_h^m \times \widehat{V}_h^m (1 \le m \le 3)$.

m		$\|e_u\|_{L^2(\Omega)}$	Order	$\|\|\|e_u\|\|\|_u$	Order	$\|e_{\mathbf{p}}\|_{L^2(\Omega)}$	Order	$\|\|\|e_{\mathbf{p}}\|\|\|_{\mathbf{p}}$	Order
1	1	4.5059e-03	-	1.5490e-01	-	3.9382e-02	-	4.2524e-02	-
	2	1.3528e-03	1.73	7.7746e-02	0.99	1.8681e-02	1.07	2.5539e-02	0.73
	3	4.0795e-04	1.73	3.8900e-02	1.00	9.3165e-03	1.00	1.5859e-02	0.68
	4	1.3376e-04	1.61	1.9563e-02	1.00	4.5537e-03	1.03	9.9689e-03	0.67
	5	5.2105e-05	1.36	9.7263e-03	1.00	2.2927e-03	1.00	6.2815e-03	0.67
2	1	2.2627e-03	-	9.3186e-03	-	3.4672e-02	-	5.1619e-02	-
	2	6.8183e-04	1.73	2.6548e-03	1.81	1.6061e-02	1.11	2.9373e-02	0.81
	3	2.3956e-04	1.51	9.2329e-04	1.52	8.0869e-03	0.99	1.8481e-02	0.67
	4	1.0011e-04	1.99	3.7505e-04	1.29	4.0509e-03	1.26	1.1383e-02	0.68
	5	4.5381e-05	1.13	1.7137e-04	1.12	2.0293e-03	1.00	7.0855e-03	0.68
3	1	2.5557e-03	-	1.1823e-02	-	4.1292e-02	-	5.7175e-02	-
	2	8.6799e-04	1.55	4.1778e-03	1.50	1.9767e-02	1.06	3.0635e-02	0.90
	3	3.3653e-04	1.36	1.4712e-03	1.50	9.6459e-03	1.03	1.0801e-02	0.76
	4	1.5550e-04	1.13	5.9787e-04	1.29	4.9361e-05	0.98	1.1136e-02	0.68
	5	7.5031e-05	1.06	2.8188e-04	1.08	2.5011e-05	0.99	6.9361e-03	0.68

and the Dirichlet function g and the source term f are taken suitably. We use the spaces $\mathbf{U}_h^m \times \widehat{V}_h^m (1 \le m \le 3)$ to approximate $\mathbf{p}$ and u, respectively. The numerical results are presented in Table 7. We still observe the optimal convergence rate for $\mathbf{p}_h$ under the L^2 norm when m is odd, and all computed convergence orders agree with the theoretical analysis.

5.2. Condition number. Here we compute the condition number of the stiffness matrix coming from the flux equation (4.3). Since the bilinear form $a_h^{\mathbf{p}}(\cdot,\cdot)$ only involves the first-order differential operator, we may expect the condition number to grow like $O(h^{-2})$. In Figure 5, we show the condition number of the stiffness matrix for both two and three dimensions. The meshes are taken from Examples 1 and 5 for the two- and three-dimensional cases, respectively. Clearly, the growth of the condition number of the stiffness matrix is shown to be $O(h^{-2})$. The theoretical analysis of the condition number may be considered as a future work.

5.3. Efficiency comparison. The number of DOFs of a discretized system is a suitable indicator for the efficiency, as illustrated by Hughes et al. in [21]. In our

TABLE 7

Example 5. *The errors* $e_u = u - u_h$, $e_{\mathbf{p}} = \mathbf{p} - \mathbf{p}_h$, *and the orders of convergence with the spaces* $\mathbf{U}_h^m \times \widehat{V}_h^m (1 \le m \le 3)$.

m		$\|e_u\|_{L^2(\Omega)}$	Order	$\|\|\|e_u\|\|\|_u$	Order	$\|e_{\mathbf{p}}\|_{L^2(\Omega)}$	Order	$\|\|\|e_{\mathbf{p}}\|\|\|_{\mathbf{p}}$	Order
	1	2.0159e-01	-	2.6227e-00	-	1.4772e-00	-	2.0737e+01	-
	2	6.7739e-02	1.76	1.4117e-00	0.89	4.3453e-01	1.80	1.0927e+01	0.93
1	3	1.8200e-02	1.90	7.3125e-01	0.95	1.1641e-02	1.90	5.4683e+00	0.99
	4	4.6456e-03	1.96	3.6691e-01	1.00	2.9923e-02	1.96	2.7331e+00	1.00
	1	2.8293e-02	-	7.6111e-01	-	3.6002e-01	-	7.0288e+00	-
	2	9.1341e-02	1.63	2.2963e-01	1.73	1.0421e-01	1.79	1.7895e+00	1.97
2	3	2.5926e-03	1.82	6.1281e-02	1.91	2.8129e-02	1.89	4.6372e-01	1.95
	4	6.8012e-04	1.93	1.5021e-02	2.01	7.2823e-03	1.95	1.1599e-01	2.00
	1	7.2877e-03	-	1.8326e-01	-	1.7658e-01	-	3.0434e+00	-
	2	7.3997e-04	3.30	2.1873e-02	3.06	1.3510e-02	3.71	3.9250e-01	2.96
3	3	5.6061e-05	3.73	2.7168e-03	3.28	9.2336e-04	3.87	5.1203e-02	3.01
	4	3.6203e-06	3.96	3.3962e-04	3.17	5.9170e-05	3.96	6.4123e-03	3.00

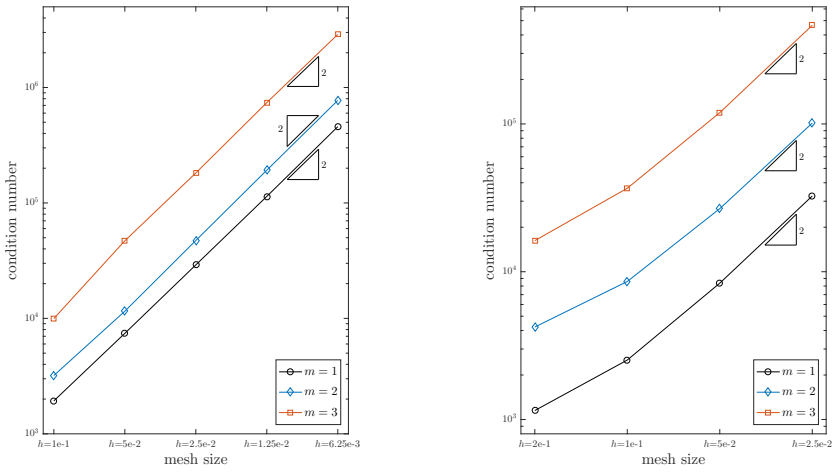

FIG. 5. *The condition number of the two-dimensional case (left)/three-dimensional case (right).*

method, the accuracy of $\mathbf{p}_h$ determines the convergence behavior of the pressure. Thus, to show the efficiency of the proposed method, we make a comparison between the standard least squares discontinuous finite element method presented in section 2 and the proposed method by comparing the error of the numerical flux $\mathbf{p}_h$.

For both methods, we select the finite element spaces of equal order for solving the Poisson problem. Here we solve the problems that are taken from Examples 1 and 5 for the two- and three-dimensional cases, respectively. We implement the two methods on successively refined meshes. In Figure 6, we plot the errors of numerical flux in the DLS energy norm $\|\cdot\|_{\mathbf{p}}$ against the number of DOFs with $1 \le m \le 3$ in two and three dimensions. All convergence orders are in perfect agreement with the theoretical results.

There are two points notable for us. To achieve the same accuracy, the proposed method uses many fewer DOFs than the DLS finite element method. The saving of the number of DOFs is more remarkable for higher-order approximation. For $d = 2$,

the number of DOFs used in our method is about 36% of that in the DLS method for linear approximation to achieve the same accuracy. Meanwhile, the number of DOFs used in our method is about 31% and 27% of the number of DOFs used in DLS method for $m = 2$ and 3, respectively (see Figure 6). In Figure 6, one may see that the saving of the number DOFs for three-dimensional problems is even more significant than for two-dimensional problems. For $d = 3$, the percentages of the number of DOFs reduce to about 30%, 12%, and 5% of that in DLS method for $m = 1$, 2, and 3, respectively.

Let us note finally that the numerical flux $\mathbf{p}_h$ obtained by our method is locally irrotational, which is a natural property as the gradient of a function.

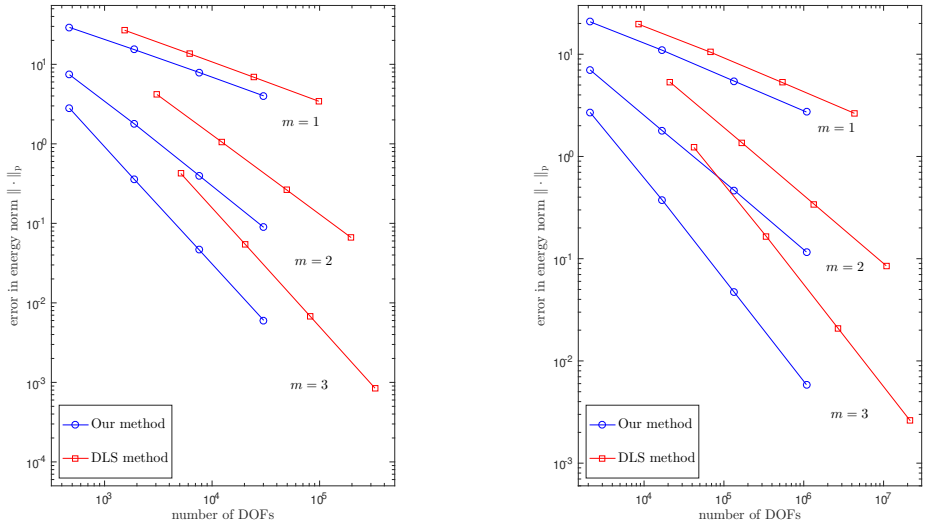

FIG. 6. *Comparison of the error* $\|\mathbf{p} - \mathbf{p}_h\|_{\mathbf{p}}$ *in the number of DOFs by two methods with* $m = 1, 2, 3$ *in two dimensions (left) and three dimensions (right).*

6. Conclusion. We proposed a sequential least squares finite element method for the Poisson equation. The novel piecewisely irrotational approximation space is constructed by solving the local least squares problem, and we use this space to decouple the least squares minimization problem. We proved the convergences for pressure and flux in the L^2 norm and energy norm. By a series of numerical results, not only are the error estimates verified, but we also exhibited the flexibility and the great efficiency of our method.

Appendix A. Here we present some details of the reconstruction process. We first give an example of constructing the element patch in the two-dimensional case. For element K, the construction of $S(K)$ with $\#S(K) = 15$ is presented in Figure 7. Further, we give some details about the computer implementation of the reconstructed space. We take the case $d = 2$ to illustrate. We first outline the bases of the space $\mathbf{S}_m(D)$; it is easily verified that for $d = 2$,

$$\mathbf{S}_1(D) = \left\{ \begin{pmatrix} 1 \\ 0 \end{pmatrix}, \begin{pmatrix} 0 \\ 1 \end{pmatrix}, \begin{pmatrix} x \\ 0 \end{pmatrix}, \begin{pmatrix} 0 \\ y \end{pmatrix}, \begin{pmatrix} y \\ x \end{pmatrix} \right\}.$$

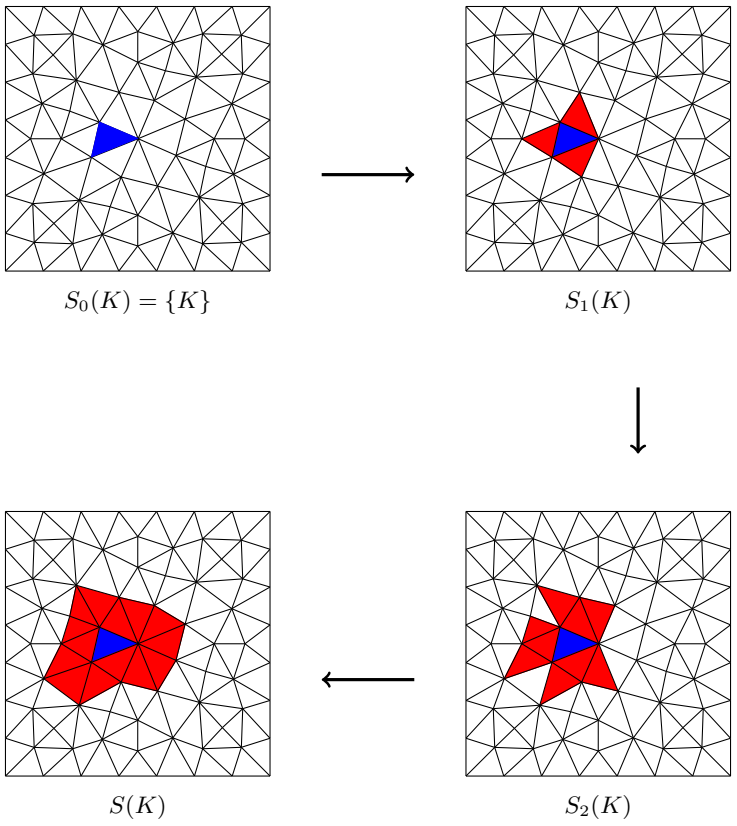

FIG. 7. *Build patch for element K with $\#S(K) = 15$.*

Similarly for $m = 2, 3$, there is

$$\mathbf{S}_2(D) = \mathbf{S}_1(D) \cup \left\{ \begin{pmatrix} x^2 \\ 0 \end{pmatrix}, \begin{pmatrix} 2xy \\ x^2 \end{pmatrix}, \begin{pmatrix} y^2 \\ 2xy \end{pmatrix}, \begin{pmatrix} 0 \\ y^2 \end{pmatrix} \right\},$$
$$\mathbf{S}_3(D) = \mathbf{S}_2(D) \cup \left\{ \begin{pmatrix} x^3 \\ 0 \end{pmatrix}, \begin{pmatrix} 3x^2 \\ y \end{pmatrix}, \begin{pmatrix} 2xy^2 \\ 2x^2y \end{pmatrix}, \begin{pmatrix} y^3 \\ 3xy^2 \end{pmatrix}, \begin{pmatrix} 0 \\ y^3 \end{pmatrix} \right\}.$$

Then we shall solve the least squares problem (3.2) on every element. We take K_0 and $m = 1$, for instance (see Figure 8), and we let $S(K_0) = \{K_0, K_1, K_2, K_3\}$, where $K_i (i = 1, 2, 3)$ are the adjacent edge-neighboring elements of K_0. We denote by $\boldsymbol{x}_i = (x_i, y_i)$ the barycenter of the element K_i, and we obtain the collocation point set $\mathcal{I}_{K_0} = \{\boldsymbol{x}_0, \boldsymbol{x}_1, \boldsymbol{x}_2, \boldsymbol{x}_3\}$.

Then for the function $\mathbf{g} = (g^1, g^2) \in \mathbf{C}^0(\Omega) \cap H(\mathrm{curl}^0; \Omega)$ the least squares problem on K_0 reads as

$$\arg\min_{\boldsymbol{a} \in \mathbb{R}^5} \sum_{i=0}^{3} \left\| a_0 \begin{pmatrix} 1 \\ 0 \end{pmatrix} + a_1 \begin{pmatrix} 0 \\ 1 \end{pmatrix} + a_2 \begin{pmatrix} x_i \\ 0 \end{pmatrix} + a_3 \begin{pmatrix} 0 \\ y_i \end{pmatrix} + a_4 \begin{pmatrix} y_i \\ x_i \end{pmatrix} - \begin{pmatrix} g^1(x_i) \\ g^2(y_i) \end{pmatrix} \right\|^2.$$

It is easy to obtain its unique solution

$$\boldsymbol{a} = (A^T A)^{-1} A^T \boldsymbol{q},$$

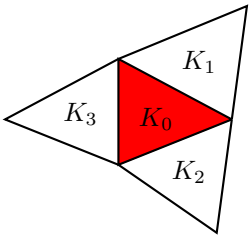

FIG. 8. *K and its neighbors.*

where

$$A = \begin{bmatrix} 1 & 0 & x_0 & 0 & y_0 \\ 0 & 1 & 0 & y_0 & x_0 \\ 1 & 0 & x_1 & 0 & y_1 \\ 0 & 1 & 0 & y_1 & x_1 \\ 1 & 0 & x_2 & 0 & y_2 \\ 0 & 1 & 0 & y_2 & x_2 \\ 1 & 0 & x_3 & 0 & y_3 \\ 0 & 1 & 0 & y_3 & x_3 \end{bmatrix}, \qquad \boldsymbol{q} = \begin{bmatrix} g^1(x_0) \\ g^2(y_0) \\ g^1(x_1) \\ g^2(y_1) \\ g^1(x_2) \\ g^2(y_2) \\ g^1(x_3) \\ g^2(y_3) \end{bmatrix}.$$

We notice that the matrix $(A^TA)^{-1}A^T$ is independent of the function $\mathbf{g}$ and includes all information of the function $\boldsymbol{\lambda}^i_{K_j}(j = 0, 1, 2, 3,\ i = 1, 2)$ on the element K_0. From (3.3), we could just store the matrix $(A^TA)^{-1}A^T$ for every element to represent our approximation space. The idea of the implementation could be adapted to the high-order accuracy case and the high-dimensional problem without any difficulty.

Acknowledgment. The authors would like to thank the anonymous referees sincerely for their constructive comments that improved the paper.

REFERENCES

[1] P. F. ANTONIETTI, L. BEIRÃO DA VEIGA, AND M. VERANI, *A mimetic discretization of elliptic obstacle problems*, Math. Comp., 82 (2013), pp. 1379–1400, https://doi.org/10.1090/S0025-5718-2013-02670-1.

[2] D. N. ARNOLD, *An interior penalty finite element method with discontinuous elements*, SIAM J. Numer. Anal., 19 (1982), pp. 742–760, https://doi.org/10.1137/0719052.

[3] D. N. ARNOLD, F. BREZZI, B. COCKBURN, AND L. D. MARINI, *Unified analysis of discontinuous Galerkin methods for elliptic problems*, SIAM J. Numer. Anal., 39 (2002), pp. 1749–1779, https://doi.org/10.1137/S0036142901384162.

[4] B. AYUSO DE DIOS, F. BREZZI, O. HAVLE, AND L. D. MARINI, *L^2-estimates for the DG IIPG-0 scheme*, Numer. Methods Partial Differential Equations, 28 (2012), pp. 1440–1465, https://doi.org/10.1002/num.20687.

[5] A. K. AZIZ, R. B. KELLOGG, AND A. B. STEPHENS, *Least squares methods for elliptic systems*, Math. Comp., 44 (1985), pp. 53–70, https://doi.org/10.2307/2007792.

[6] R. BENSOW AND M. G. LARSON, *Discontinuous least-squares finite element method for the div-curl problem*, Numer. Math., 101 (2005), pp. 601–617, https://doi.org/10.1007/s00211-005-0600-y.

[7] R. E. BENSOW AND M. G. LARSON, *Discontinuous/continuous least-squares finite element methods for elliptic problems*, Math. Models Methods Appl. Sci., 15 (2005), pp. 825–842, https://doi.org/10.1142/S0218202505000595.

[8] P. BOCHEV, J. LAI, AND L. OLSON, *A locally conservative, discontinuous least-squares finite element method for the Stokes equations*, Internat. J. Numer. Methods Fluids, 68 (2012), pp. 782–804, https://doi.org/10.1002/fld.2536.

[9] P. Bochev, J. Lai, and L. Olson, *A non-conforming least-squares finite element method for incompressible fluid flow problems*, Internat. J. Numer. Methods Fluids, 72 (2013), pp. 375–402, https://doi.org/10.1002/fld.3748.

[10] P. B. Bochev and M. D. Gunzburger, *Accuracy of least-squares methods for the Navier-Stokes equations*, Comput. & Fluids, 22 (1993), pp. 549–563, https://doi.org/10.1016/0045-7930(93)90025-5.

[11] P. B. Bochev and M. D. Gunzburger, *Finite element methods of least-squares type*, SIAM Rev., 40 (1998), pp. 789–837, https://doi.org/10.1137/S0036144597321156.

[12] P. B. Bochev and M. D. Gunzburger, *Least-Squares Finite Element Methods*, Appl. Math. Sci. 166, Springer, New York, 2009, https://doi.org/10.1007/b13382.

[13] J. H. Bramble, R. D. Lazarov, and J. E. Pasciak, *A least-squares approach based on a discrete minus one inner product for first order systems*, Math. Comp., 66 (1997), pp. 935–955, https://doi.org/10.1090/S0025-5718-97-00848-X.

[14] C. L. Chang, *An error estimate of the least squares finite element method for the Stokes problem in three dimensions*, Math. Comp., 63 (1994), pp. 41–50, https://doi.org/10.2307/2153561.

[15] P. G. Ciarlet, *The Finite Element Method for Elliptic Problems*, Classics Appl. Math. 40, SIAM, Philadelphia, 2002, https://doi.org/10.1137/1.9780898719208; reprint of the original, North–Holland, Amsterdam, 1978.

[16] D. Di Pierto, A. Ern, and S. Lemaire, *An arbitrary-order and compact-stencil discretization of diffusion on general meshes based on local reconstruction operators*, Comput. Methods Appl. Math., 14 (2014), pp. 461–472.

[17] V. Dolejší and O. Havle, *The L^2-optimality of the IIPG method for odd degrees of polynomial approximation in 1D*, J. Sci. Comput., 42 (2010), pp. 122–143, https://doi.org/10.1007/s10915-009-9319-8.

[18] E. H. Georgoulis and T. Pryer, *Recovered finite element methods*, Comput. Methods Appl. Mech. Engrg., 332 (2018), pp. 303–324, https://doi.org/10.1016/j.cma.2017.12.026.

[19] C. Geuzaine and J. F. Remacle, `Gmsh`*: A 3-D finite element mesh generator with built-in pre- and post-processing facilities*, Internat. J. Numer. Methods Engrg., 79 (2009), pp. 1309–1331, https://doi.org/10.1002/nme.2579.

[20] V. Girault and P. A. Raviart, *Finite Element Methods for Navier-Stokes Equations: Theory and Algorithms*, Springer-Verlag, Berlin, Heidelberg, 1986, http://doi.org/10.1007/978-3-642-61623-5.

[21] T. J. R. Hughes, G. Engel, L. Mazzei, and M. G. Larson, *A comparison of discontinuous and continuous Galerkin methods based on error estimates, conservation, robustness and efficiency*, in Discontinuous Galerkin Methods (Newport, RI, 1999), Lect. Notes Comput. Sci. Eng. 11, Springer, Berlin, 2000, pp. 135–146, https://doi.org/10.1007/978-3-642-59721-3_9.

[22] B.-N. Jiang and L. A. Povinelli, *Optimal least-squares finite element method for elliptic problems*, Comput. Methods Appl. Mech. Engrg., 102 (1993), pp. 199–212, https://doi.org/10.1016/0045-7825(93)90108-A.

[23] M. G. Larson and A. J. Niklasson, *Analysis of a family of discontinuous Galerkin methods for elliptic problems: The one dimensional case*, Numer. Math., 99 (2004), pp. 113–130, https://doi.org/10.1007/s00211-004-0528-7.

[24] K. Larsson and M. Larson, *Continuous piecewise linear finite elements for the Kirchhoff-Love plate equation*, Numer. Math., 121 (2012), pp. 65–97.

[25] R. Li, P. Ming, Z. Sun, and Z. Yang, *An arbitrary-order discontinuous Galerkin method with one unknown per element*, J. Sci. Comput., 80 (2019), pp. 268–288, https://doi.org/10.1007/s10915-019-00937-y.

[26] R. Li, P. B. Ming, Z. Y. Sun, F. Y. Yang, and Z. J. Yang, *A discontinuous Galerkin method by patch reconstruction for biharmonic problem*, J. Comput. Math., 37 (2019), pp. 561–578.

[27] R. Li, P. Ming, and F. Tang, *An efficient high order heterogeneous multiscale method for elliptic problems*, Multiscale Model. Simul., 10 (2012), pp. 259–283, https://doi.org/10.1137/110836626.

[28] W. F. Mitchell, *A collection of 2D elliptic problems for testing adaptive grid refinement algorithms*, Appl. Math. Comput., 220 (2013), pp. 350–364, https://doi.org/10.1016/j.amc.2013.05.068.

[29] W. F. Mitchell, *How high a degree is high enough for high order finite elements?*, Procedia Comput. Sci., 51 (2015), pp. 246–255, https://doi.org/10.1016/j.procs.2015.05.235.

[30] L. Mu, J. Wang, and X. Ye, *A least-squares-based weak Galerkin finite element method for second order elliptic equations*, SIAM J. Sci. Comput., 39 (2017), pp. A1531–A1557, https://doi.org/10.1137/16M1083244.

[31] A. I. Pehlivanov, G. F. Carey, and R. D. Lazarov, *Least-squares mixed finite elements for second-order elliptic problems*, SIAM J. Numer. Anal., 31 (1994), pp. 1368–1377, https://doi.org/10.1137/0731071.

[32] C. Talischi, G. H. Paulino, A. Pereira, and I. F. M. Menezes, `PolyMesher`*: A general-purpose mesh generator for polygonal elements written in MATLAB*, Struct. Multidiscip. Optim., 45 (2012), pp. 309–328, https://doi.org/10.1007/s00158-011-0706-z.

[33] X. Ye and S. Zhang, *A discontinuous least-squares finite-element method for second-order elliptic equations*, Int. J. Comput. Math., 96 (2019), pp. 557–567, https://doi.org/10.1080/00207160.2018.1445230.

[34] O. C. Zienkiewicz, R. L. Taylor, S. J. Sherwin, and J. Peiró, *On discontinuous Galerkin methods*, Internat. J. Numer. Methods Engrg., 58 (2003), pp. 1119–1148, https://doi.org/10.1002/nme.884.